Solid State Communications 351 (2022) 114788

Contents lists available at ScienceDirect

Solid State Communications

journal homepage: www.elsevier.com/locate/ssc

Characterisation of optical phonons within epitaxial $Ge_2Sb_2Te_5$/InAs (111) structures

R.A. Alsaigh [a,b], L.R. Shelford [a], H.J. Mohamad [a], A. Shalini [a], U.A.S. Al-Jarah [a], V. Bragaglia [c,1], A. Giussani [c], R. Calarco [c,d], G.P. Srivastava [a], R.J. Hicken [a,*]

[a] Department of Physics and Astronomy, Stocker Road, University of Exeter, Exeter, EX4 4QL, UK
[b] Department of Physics and Astronomy, King Saud University, Riyadh, 11451, Saudi Arabia
[c] Paul-Drude-Institut für Festkörperelektronik, Hausvogteiplatz 5-7, 10117, Berlin, Germany
[d] Instituto per La Microelettronica e Microsistemi (IMM), Consiglio Nazionale delle Ricerche (CNR), Via del Fosso del Cavaliere, 100, 00133, Rome, Italy

ARTICLE INFO

Communicated by F. Peeters

Keywords:
GST225
Ultrafast pump-probe
Coherent phonon

ABSTRACT

Femto-second pump-probe and micro-Raman spectroscopy (RS) measurements have been made to identify optical phonons in $Ge_2Sb_2Te_5$/InAs(111) and an InAs(111) substrate. A theory of transient stimulated Raman scattering (TSRS) incorporating the Raman tensor predicts which phonon modes may be observed in transient reflectance (R) and anisotropic reflectance (AR) pump-probe measurements, and how their amplitudes depend upon angles φ and θ that describe the orientation of the pump and probe beam electric fields within the sample plane. AR measurements of an InAs(111) substrate revealed the 6.5 THz T_2 transverse optical phonon with amplitude proportional to sin(2(θ−φ)), as expected for both TSRS and the specular optical Kerr effect (SOKE), confirming that TSRS and SOKE are equivalent descriptions of the same phenomenon. The AR responses of $Ge_2Sb_2Te_5$/InAs(111) revealed a single coherent optical phonon (COP) mode at about 3.4 THz with sin(2(θ−φ)) amplitude variation that confirms the T_2-like character of the mode and hence the underlying cubic structure of the epilayer. This mode was also observed in the R measurement for one sample, with amplitude independent of φ and θ as predicted by TSRS theory. Both R and AR signals were heavily damped, which is attributed to dephasing of T_{2x}, T_{2y} and T_{2z} modes that become non-degenerate due to structural distortions. RS measurements revealed three modes for $Ge_2Sb_2Te_5$/InAs(111) and three modes for InAs(111). Taken together the TSRS and RS measurements provide rich information about optical phonons in the phase change material $Ge_2Sb_2Te_5$ and the InAs(111) surface.

1. Introduction

Phase change materials (PCMs) possess optical and electrical properties that make them of great interest for technological applications [1]. The most commonly used and most studied PCM is $Ge_2Sb_2Te_5$ (GST), due firstly to the fast and reversible phase transition that occurs between its amorphous and crystalline phases, and secondly to the strong difference in optical reflectance and electrical resistivity between these two phases. X-ray diffraction (XRD) studies of thin film GST show that the GST layer crystallizes into a metastable rocksalt-like structure with Te atoms occupying the anion sites of the face-centred cubic (fcc) structure. The cation sites are either occupied by Ge and Sb atoms or are vacant [2]. The distribution of vacancies and structure of GST has been intensively studied and it is believed that Ge atoms coexist with octahedral and tetrahedral coordination [3]. The investigation of coherent optical phonons can provide insight into both the structure and the structural phase transition that occurs within the material. Furthermore, the investigation of epitaxial GST films can yield improved understanding of the character of the phonon spectrum since the orientation of pump and probe electric field relative to the crystallographic axes of the sample can be carefully controlled [4].

Theoretical and experimental studies have been performed of the long wavelength phonon modes of GST. For crystalline fcc-GST, degenerate E_g modes with frequency of 3.6 ± 0.1 THz have been observed [5–7]. These modes have been compared to the vibration of atoms in planes normal to the c-axis in Sb_2Te_3 [5,6,8]. In contrast, this

* Corresponding author.
E-mail address: r.j.hicken@exeter.ac.uk (R.J. Hicken).
[1] Present address IBM Research-Zurich Säumerstrasse 4 CH–8803 Rüschlikon Switzerland.

https://doi.org/10.1016/j.ssc.2022.114788
Received 6 December 2021; Received in revised form 2 April 2022; Accepted 6 April 2022
Available online 20 April 2022

frequency corresponds to that of an A_1 mode in $GeTe_4$ [9] and in octahedral $GeTe_6$ [10]. Two A_{1g} modes appear at 2 THz and at 4.9 ± 0.1 THz for fcc-GST. These two modes are attributed to symmetrical vibrations of Sb and Te outer layers, where the mode at 2 THz is due to an in-phase oscillation [5] while the mode at 4.9 ± 0.1 THz is due to an out of phase oscillation [5,6]. For the amorphous phase of GST, a dominant symmetrical A_1 mode at 3.7 ± 0.2 THz was observed and associated with $GeTe_4$ tetrahedra [5,6,10]. Also a symmetric A_1 mode appears at 4.7 ± 0.1 THz and has been attributed to either disordered Te–Te chains [10] or Sb_2Te_3 sub-units [5].

Theoretical studies have been made of the Raman spectra of cubic GST material from *ab-initio* phonon and empirical polarizability coefficients within the bond polarizability model (BPM) [11]. Two modes are predicted in crystalline GST, one at 110 cm^{-1} (3.29 THz) and another weaker mode at 160 cm^{-1} (4.79 THz). However, the same study also considered amorphous GST and predicted two modes at 129 cm^{-1} (3.86 THz) and 152 cm^{-1} (4.55 THz), and a much weaker mode at 100 cm^{-1} (2.99 THz). A calculation of the Raman spectrum of amorphous GST predicted one mode at 143 cm^{-1} (4.2 THz) and a shoulder at 160 cm^{-1} (4.79 THz), both of which were attributed to vibrations of defective octahedra [11]. Broadly speaking, theory and experiment find modes within the frequency ranges 3.3–3.9 and 4.2–4.9 THz, for cubic and amorphous GST, but with some variation in the precise values of the frequencies between different studies.

A variety of optical and THz measurement techniques have been used to probe the electrical and vibrational properties of GST [4,12–14]. Optical pump-probe measurements allow coherent optical phonons (COPs) to be studied by transient stimulated Raman scattering (TSRS) [15]. A theory of TSRS allows the dependence of the pump-probe signal upon the pump and probe polarisation to be determined. [16] This theory was previously applied to a study of GST/GaSb(001) [4]. Two optical phonons were observed in the anisotropic reflectance (AR) signal, a mode at 3.4 THz belonging to the GST layer and another mode at 6.7 THz belonging to the GaSb substrate. The study revealed a four-fold dependence of the amplitude of the 3.4 THz mode upon the probe polarisation but only a weak dependence upon pump polarisation. The TSRS theory predicts that only the A and E modes should be observed in the reflectance (R) signal, with no dependence upon pump and probe polarisation. Only the T_{2z} mode [17] should be observed in the AR signal, with amplitude proportional to $\sin(2\varphi)\cos(2\theta)$, where the electric field of pump and probe lie in the (001) plane and describe angles φ and θ respectively with the [100] axis. Therefore, the detection of the 3.4 THz COP and the dependence of its amplitude upon probe polarisation can be used to infer T_2-like character. However, excitation most likely occurs by the generation of a space charge (SC) electric field, since no obvious dependence of the amplitude upon the pump polarisation was observed. The 3.4 THz COP has the character of the three dimensional T_2 mode of the rock-salt structure, and its observation confirms that the underlying crystallographic structure of GST is cubic. Note that the T_2 mode is Raman inactive in defect-free rocksalt structure, but becomes Raman active in defective or distorted rocksalt structure, such as cubic GST.

In this work, time-resolved R and AR measurements are presented of coherent optical phonons (COPs) within an InAs(111) wafer and epitaxial GST/InAs(111). It has been found that GST(111) films grown on Si(111) and InAs(111) substrates exhibit improved structural quality compared to GST(001) grown on Si(001) and InAs(001) [18], [19], while measurements made on GST(111) provide a test of the TSRS theory developed to describe measurements performed on GST(001) films. The termination of the InAs surface (In or As rich) and its surface reconstruction can influence the structural quality of the GST film [20,21], while steps on the substrate surface may induce additional strain [22]. With this in mind, results from two $Ge_2Sb_2Te_5$/InAs(111) samples (grown on different substrates, and labelled A and B) are compared to explore reproducibility given the sensitivity to growth conditions. The orientation of pump and probe electric field directions are varied relative to one another and relative to the crystallographic axes. Micro Raman measurements are presented to identify all Raman active modes and to verify the modes detected by the pump–probe measurements. In addition, changes to the observed modes, resulting from structural changes induced by large optical pump power, are explored. The results are interpreted using microscopic and macroscopic Raman theories as well as a theory of transient stimulated Raman scattering (TSRS) based upon use of the Raman tensor.

1.1. Experiment

Optical pump-probe measurements were performed upon a 350 μm thick InAs(111) wafer and two GST(20, 22 nm)/InAs(111) samples prepared by molecular beam epitaxy [18,19,23,24]. Measurements were made with a Ti:sapphire laser amplifier system at 800 nm wavelength, with 45 fs pulse duration and a repetition rate of 100 KHz. The pump beam was at near to normal incidence and had linear polarisation that could be oriented in any direction within the plane of the sample, while the s-polarised probe beam was incident at 45° to the sample normal. The reflected probe beam was directed through a quarter wave plate and into a balanced polarisation bridge detector consisting of a polarizing beam splitter and two photodiodes. The sum and difference of the photodiode outputs yielded the transient R and AR (ellipticity) signals respectively [4]. Ellipticity was measured instead of rotation because the ellipticity signal, and hence the signal to noise ratio, was found to be larger in the case of the GST samples. An optical chopper was placed in the pump beam and two lock-in amplifiers used to record signals in a phase sensitive manner.

Four different sets of measurements were made. Firstly, measurements were made as the pump polarisation was rotated through 180° while the probe beam had s-polarisation. Secondly, measurements were made as the sample was rotated about its normal with the direction of the pump and probe polarisation 45° apart. Third, measurements were made as the sample orientation and pump beam polarisation were rotated together while the probe polarisation was fixed. Finally, measurements were made to explore the effect of pump fluence on R and AR signals with the pump and probe polarisation set 45° apart. Measurements made at high pump fluence were then immediately repeated at a lower fluence to determine whether an irreversible change of the sample response had occurred. Micro Raman measurements were also performed on all three samples.

1.2. Theory

A theory of transient stimulated Raman scattering (TSRS) was used to determine the expected dependence of the R and AR signals due to the COPs upon the pump and probe polarisation. The pump beam can excite COPs either by impulsive stimulated Raman scattering (ISRS), or by generation of a space charge (SC) field where the electrons and holes become spatially separated due either to the electric field created near an interface, or due to the photo Dember effect whereby electrons and holes diffuse at different rates due to their different mobilities. The change in the reflectivity of the material induced by the COPs is assumed to be small with respect to the unperturbed reflectivity, so that the transient reflectance ΔR/R detected by the probe is given by [4],

$$\frac{\Delta R}{R} \sim \left(C + \sum_{mp} \frac{\partial \chi_{mp}}{\partial Q} \cos(\alpha_m)\cos(\alpha_p) \right) \times \left(\sum_{kl} \frac{\partial \chi_{kl}}{\partial Q} \cos(\beta_k)\cos(\beta_l) \right), \quad (1)$$

where $\cos(\alpha_m)$ and $\cos(\alpha_p)$, and $\cos(\beta_k)$ and $\cos(\beta_l)$ are the direction cosines of the pump and probe electric field respectively, $\frac{\partial \chi}{\partial Q}$ is the Raman tensor, χ_{mp} is the susceptibility of the material, Q is the phonon

Table 1
Expected dependence of amplitude of S_R and S_{AR} signals due to ISRS upon pump and probe polarisation for rock salt and zinc blende films of (001) and (111) orientation. The electric field of pump and probe lie within the plane of the film. The electric field of the pump (probe) describes angle φ (θ) with the [100] and [1$\bar{1}$0] axes of films of (001) and (111) orientation respectively.

Mode	Transient Reflectivity S_R		Transient Anisotropic Reflectivity S_{AR}	
	(001)	(111)	(001)	(111)
A	a^2	a^2	0	0
E	a^2	a^2	0	0
E	a^2	a^2	0	0
T_{2x}	0	$-\frac{2}{3}d\left(\frac{1}{\sqrt{3}}d\sin 2\varphi - \frac{2}{3}d\sin^2\varphi\right)$	0	$\left(\frac{1}{\sqrt{3}}d\sin 2\varphi - \frac{2}{3}d\sin^2\varphi\right)\left(\frac{2}{\sqrt{3}}d\cos 2\theta - \frac{2}{3}d\sin 2\theta\right)$
T_{2y}	0	$-\frac{2}{3}d\left(\frac{-1}{\sqrt{3}}d\sin 2\varphi - \frac{2}{3}d\sin^2\varphi\right)$	0	$\left(\frac{-1}{\sqrt{3}}d\sin 2\varphi - \frac{2}{3}d\sin^2\varphi\right)\left(\frac{-2}{\sqrt{3}}d\cos 2\theta - \frac{2}{3}d\sin 2\theta\right)$
T_{2z}	0	$-\frac{2}{3}d\left(-d\cos^2\varphi + \frac{1}{3}d\sin^2\varphi\right)$	$d^2\sin(2\varphi)\cos(2\theta)$	$\left(-d\cos^2\varphi + \frac{1}{3}d\sin^2\varphi\right)\left(-\frac{4}{3}d\sin 2\theta\right)$

displacement, and C represents the contribution of the SC field to the excitation.

If the pump and probe electric fields lie within the (111) plane and describe angles φ and θ respectively with the [1$\bar{1}$0] axis, then

$$\mathbf{E}_{pump} = \mathrm{E}_{pump}(cos\varphi\hat{\boldsymbol{u}} + sin\varphi\hat{\boldsymbol{v}}) \quad \text{and} \quad \mathbf{E}_{probe} = \mathrm{E}_{probe}(cos\theta\hat{\boldsymbol{u}} + sin\theta\hat{\boldsymbol{v}}). \tag{2}$$

with the unit vectors

$$\hat{\boldsymbol{u}} = \frac{1}{\sqrt{2}}(1,-1,0) \quad \text{and} \quad \hat{\boldsymbol{v}} = \frac{1}{\sqrt{6}}(1,1,-2)\,. \tag{3}$$

The probe beam is passed into a bridge detector that consists of a polarizing beam splitter and two photo diodes $\mathscr{A}$ and $\mathscr{B}$. The beam splitter is oriented so that the reflected probe beam is separated into two beams of orthogonal polarisation and equal intensity. Therefore the electric fields of these two beams are oriented at $\pm 45^{\circ}$ relative to that of the probe beam and may be written as

$$\mathbf{E}_{\mathscr{A}} = \frac{1}{\sqrt{2}}E_{probe}\begin{pmatrix} \frac{1}{\sqrt{2}}cos\left(\theta+\frac{\pi}{4}\right) + \frac{1}{\sqrt{6}}\sin\left(\theta+\frac{\pi}{4}\right) \\ -\frac{1}{\sqrt{2}}\cos\left(\theta+\frac{\pi}{4}\right) + \frac{1}{\sqrt{6}}\sin\left(\theta+\frac{\pi}{4}\right) \\ -\sqrt{2/3}sin\left(\theta+\frac{\pi}{4}\right) \end{pmatrix} \tag{4}$$

and

$$\mathbf{E}_{\mathscr{B}} = \frac{1}{\sqrt{2}}E_{probe}\begin{pmatrix} \frac{1}{\sqrt{2}}cos\left(\theta-\frac{\pi}{4}\right) + \frac{1}{\sqrt{6}}\sin\left(\theta-\frac{\pi}{4}\right) \\ -\frac{1}{\sqrt{2}}\cos\left(\theta-\frac{\pi}{4}\right) + \frac{1}{\sqrt{6}}\sin\left(\theta-\frac{\pi}{4}\right) \\ -\sqrt{2/3}\,sin\left(\theta-\frac{\pi}{4}\right) \end{pmatrix}. \tag{5}$$

The transient reflectance $(\Delta R/R)$ recorded by photodiodes $\mathscr{A}$ and $\mathscr{B}$ due to ISRS may be written as

$$(\Delta R/R)_{\mathscr{A}} \propto \left(\mathbf{E}^{\mathrm{T}}_{pump}\, M\, \mathbf{E}_{pump}\right)\left(\mathbf{E}^{\mathrm{T}}_{\mathscr{A}}\, M\, \mathbf{E}_{\mathscr{A}}\right) \quad \text{and} \quad (\Delta R/R)_{\mathscr{B}} \propto \left(\mathbf{E}^{\mathrm{T}}_{pump}\, M\, \mathbf{E}_{pump}\right)\left(\mathbf{E}^{\mathrm{T}}_{\mathscr{B}}\, M\, \mathbf{E}_{\mathscr{B}}\right) \tag{6}$$

where M is the matrix representing the Raman tensor for the particular phonon mode, while the detector electronics outputs the sum and difference signals

$$S_R = (\Delta R/R)_{\mathscr{A}} + (\Delta R/R)_{\mathscr{B}} \quad \text{and} \quad S_{AR} = (\Delta R/R)_{\mathscr{A}} - (\Delta R/R)_{\mathscr{B}}. \tag{7}$$

In fact, the bridge measures optical rotation, the real part of the AR signal, but a quarter wave plate may be placed in front of the detector to instead record ellipticity, the imaginary part of the AR signal.

The cubic zinc blende and rock salt structures have T_d and O_h point groups respectively, with irreducible representations A, 2E, and T_2 (T_{2x}, T_{2y}, T_{2z}). The matrix representations of the Raman tensor in each case are

$$\mathrm{A}\begin{bmatrix} a & 0 & 0 \\ 0 & a & 0 \\ 0 & 0 & a \end{bmatrix}, \mathrm{E}\begin{bmatrix} b & 0 & 0 \\ 0 & b & 0 \\ 0 & 0 & b \end{bmatrix}, \mathrm{T_{2x}}\begin{bmatrix} 0 & 0 & 0 \\ 0 & 0 & d \\ 0 & d & 0 \end{bmatrix}, \mathrm{T_{2y}}\begin{bmatrix} 0 & 0 & d \\ 0 & 0 & 0 \\ d & 0 & 0 \end{bmatrix}, \mathrm{T_{2z}}\begin{bmatrix} 0 & d & 0 \\ d & 0 & 0 \\ 0 & 0 & 0 \end{bmatrix}. \tag{8}$$

A phonon mode from one of the above representations can be detected in the R or AR signal when S_R or S_{AR} respectively are non-zero. Substituting equations (2)–(6) and Eq 8 into Eq 7yields the values for S_R and S_{AR} shown in Table 1.

The pump beam is expected to excite T_{2x}, T_{2y}, and T_{2z} phonons with equal probability. Therefore, the dependence of the measured S_R and S_{AR} signals upon pump and probe polarisation is in each case obtained by superposing the three expressions within Table 1.

The result is that, for a crystal of (111) orientation in the experimental geometry described previously, S_R is independent of the angles θ and φ, while S_{AR} varies as $\sin(2(\theta-\varphi))$. S_{AR} has maximum value when the angle between the pump and probe polarisation is 45°, and has exactly the same angular dependence as expected for the specular optical Kerr effect (SOKE).

Macroscopic and microscopic Raman theories based upon the Raman tensor and the phonon representation were used to understand which optical phonons are Raman active. An optical phonon that modifies the polarizability can be Raman active in first order Raman scattering, and requires the phonon displacement representation to be contained within the set of the point group representation. The phonon displacement vector Q can have even or odd parity under inversion. For the optical phonon mode, Q has even parity if the basis atoms vibrate with the same amplitude and phase, or has odd parity if not. For centrosymmetric crystals such as diamond and rock salt, both the atomic positions and $(\partial\chi/\partial Q)$ are invariant under inversion. For the diamond structure there are two identical basis atoms, thus Q has even parity, and so the optical phonon mode is Raman active. In the rock salt structure there are two different basis atoms, thus the phonon displacement vector Q has odd

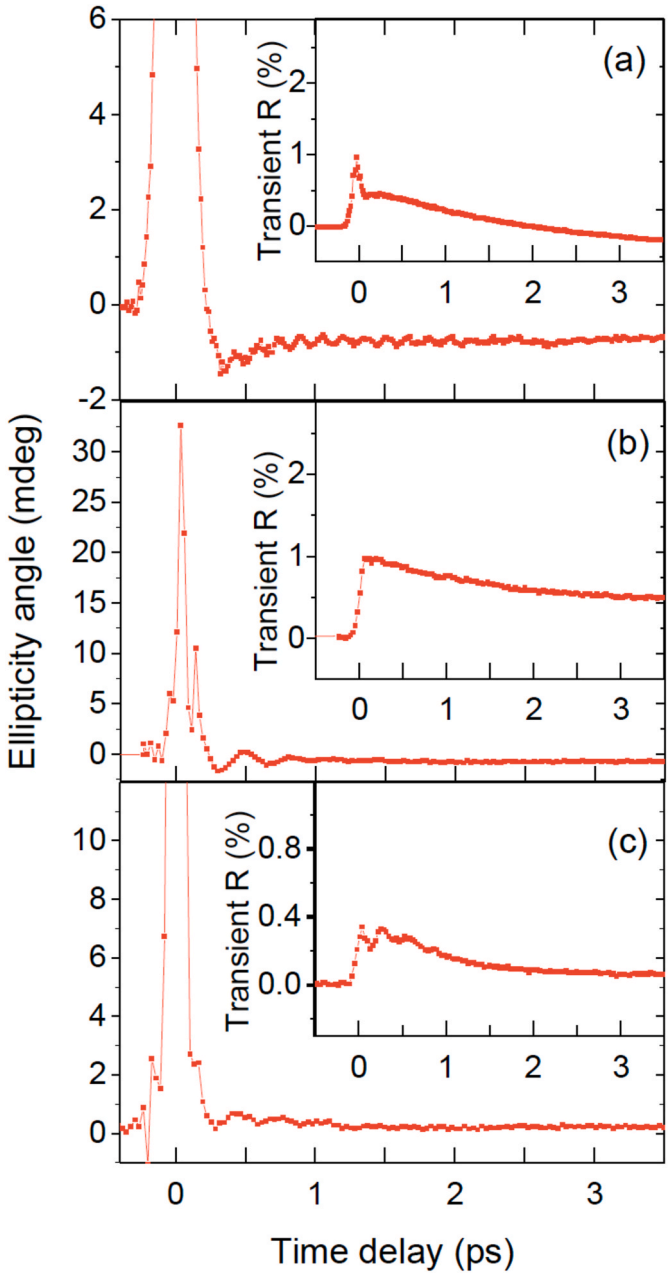

Fig. 1. Typical time resolved ellipticity (S_{AR}) and reflectivity (S_R) signals for (a) a bare InAs(111) substrate, and (b) GST/InAs(111) sample A, and (c) sample B. The pump fluence was 1.06 mJ/cm^2 in all cases.

parity, and the optical phonon mode is Raman inactive. Finally, for the zinc blende structure, which has two non-identical basis atoms and lacks inversion symmetry, $(\partial\chi/\partial Q)$ changes sign under inversion. The displacement pattern in this structure exhibits odd parity. Therefore, the optical phonon is Raman active in the zinc blende structure [25].

2. Results

Typical time-resolved R and AR (ellipticity) signals are shown in Fig. 1 for a bare InAs(111) substrate in panel (a) and for the A and B GST/InAs(111) samples in panels (b) and (c), when the electric field of the pump beam lies at 45° relative to that of the s-polarised probe beam. The form of the signals was found to depend only upon the relative orientation of the pump and probe polarisations, and to be independent of the orientation of the pump and probe electric fields relative to the crystallographic axes. The AR response of all three samples shows a clear peak at zero time delay due to the specular optical effect (SOKE). The SOKE peak is observed to have maximum amplitude when the pump and probe polarisation are set 45° apart, and zero amplitude when they are set parallel or perpendicular to each other. The SOKE peak appears because the electron momentum distribution in the sample is modified by the pump and is short lived due to the short momentum relaxation time. For the InAs(111) substrate the SOKE peak is accompanied by long lived oscillations, with relaxation time of about 1.5 ps, that are associated with a COP with frequency of 6.5 THz. For the two GST/InAs(111) samples, the SOKE peak is accompanied by oscillations, with relaxation time of about 1.75 ps, with frequency that increases gradually with increasing time during the scan. In each case the oscillations are superimposed upon a slowly decaying background. After supplying heat to the sample, the bonding between neighbouring ions is weakened, which leads to oscillations of lower frequency, but with the frequency increasing as the sample cools. Fig. 2 shows the oscillatory component of the ellipticity (AR) signal for sample A for an s-polarised probe beam as the pump beam polarisation is varied through 180° in 10° steps.

The R response presented in Fig. 1(a) shows that the initial rise of the signal occurs within a 10–90 rise time of 150 fs for the bare InAs(111) substrate, with no clear oscillations visible, and is attributed to the photoexcitation and thermalization of an electron-hole plasma. Typical transient R signals from the A and B GST/InAs(111) samples are shown in panel (b) and (c) respectively. The initial rise of the signal occurs within 125 fs for both GST/InAs(111) samples. A clear oscillation with frequency of 3.4 THz is observed only for GST/InAs (111) sample B, while no clear oscillations are seen for sample A. The transient reflectance signal of all three samples was found to be independent of pump polarisation, except in the region where the pump and probe overlap in time, where bleaching of the optical transition may occur.

The dependence of the phonon frequency and amplitude, extracted from the ellipticity (AR) signals, upon pump polarisation for all three samples is shown in Fig. 3. The decay time of the oscillations, and the width of the associated power spectrum, were found to be independent of pump polarisation within the accuracy of the measurements and fitting procedure and so have not been plotted. The amplitude is plotted as a positive quantity and so the expected analytical form $|\sin(2(\theta-\varphi))|$ is plotted for comparison. The experimental values are in reasonable agreement with the analytical form except in Fig. 2(f) where it is likely that drift in the overlap of pump and probe spots led to the measured amplitude being smaller for angles of 0°–90° compared to 90°–180°. The black symbols show the values obtained by fitting a Lorentzian curve to the peak in the fast Fourier transform (FFT) power spectrum, while the red symbols show values obtained by fitting the time domain (TD) data assuming zero chirp. The frequencies determined by these two methods are found to be in good agreement and appear to be independent of pump polarisation. The blue symbols in panels (b) and (c) show the frequencies obtained by fitting the oscillatory component of the data after background subtraction, and allowing the chirp parameter to vary. The dependence of the phonon frequencies and amplitudes, extracted from the R signals for GST/InAs(111) sample B, upon pump polarisation are shown in panels (a) and (b) of Fig. 4 respectively. The frequency and amplitude appear to be independent of pump polarisation. A structural phase transition may occur when a PCM such as GST is heated by one or more laser pulses. Therefore, the effect of pump fluence on the transient R and AR signals, and hence upon the COPs within GST/InAs (111), was studied with the pump and probe polarisations set 45° apart. A measurement was made at high pump fluence then immediately repeated at a lower pump fluence of 1.01 mJ/cm^2 for the bare InAs(111) substrate and of 0.99 mJ/cm^2 for both GST/InAs(111) samples. The R and AR signals obtained from the repeated measurements on GST/InAs(111) sample A are shown in Fig. 5, and oscillation frequencies were extracted from the FFT power spectra. At low pump fluence, oscillations associated with a COP, with frequency of about 3 THz, are observed in the AR signal but not the R signal. After exposure to a fluence of 2.97 mJ/cm^2,

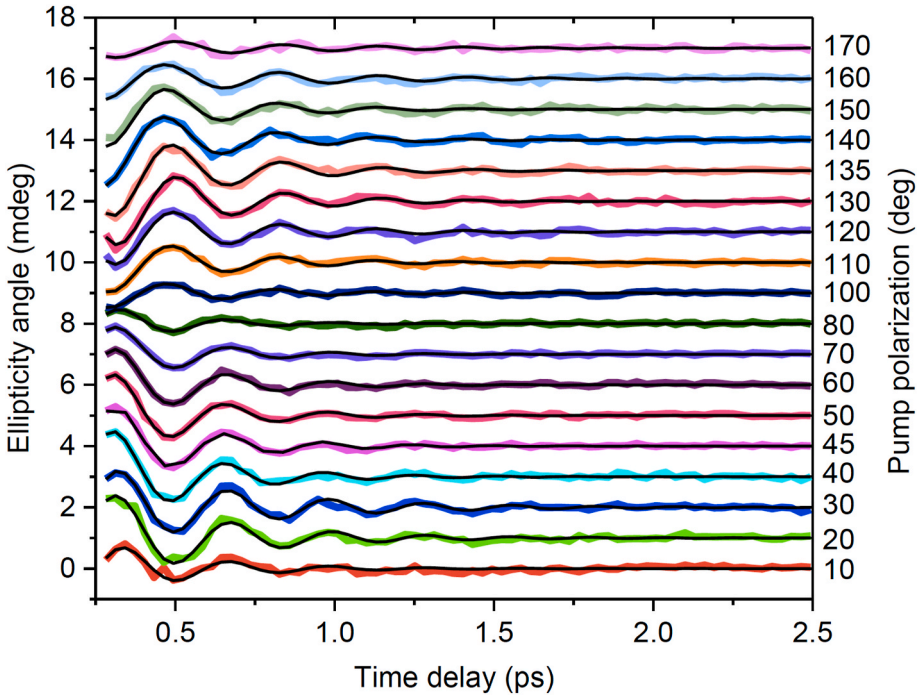

Fig. 2. Oscillatory component of the ellipticity (AR) signal obtained from sample A with an s-polarised probe beam and with the pump beam polarised relative to the probe beam at the angles shown, stated in degrees. The black curves are fits to the experimental data (coloured points) that allow for chirp.

the 3 THz mode vanishes while another COP with frequency of about 3.5 THz and larger amplitude appears in both R and AR signals. The initial phase of oscillation of the AR signal is seen to reverse as the frequency changes. Surprisingly, for sample B, exposure to high fluence had little effect. There was no increase in the phonon amplitude, in fact the amplitude decreased and there was no noticeable change in frequency. This suggests that no structural change was induced in sample B. For the bare InAs(111) substrate, repeated measurements at low fluence showed that the signal shape and oscillation frequency were unaffected by exposure to elevated pump fluence, suggesting that no structural changes had taken place. This is consistent with InAs being a harder material with a higher melting point.

Micro-Raman measurements were also performed on all samples. The Raman spectrum obtained from the bare InAs (111) substrate is shown in Fig. 6(a). The spectrum shows three peaks, one centred at about 216 cm^{-1} (6.5 THz) which can be attributed to the zone centre TO phonon, which is also detected in pump-probe measurements, and another centred at 234 cm^{-1} (7.0 THz) that can be attributed to the zone centre LO phonon [25]. In addition to the TO and LO phonon peaks there is also another peak centred at 226 cm^{-1} (6.8 THz) that can be attributed to the Fuchs-Kliewer surface optical phonon [26]. The Raman spectrum of GST/InAs(111) sample A contains a broad band between 100 and 200 cm^{-1} with three different peaks at about 122 cm^{-1} (3.7 $\pm$ 0.001 THz), 139 cm^{-1} (4.2 $\pm$ 0.003 THz) and 151 cm^{-1} (4.6 $\pm$ 0.076 THz). The peak at 216 cm^{-1} (6.5 THz) observed previously for the InAs(111) substrate is also seen. The Raman spectrum of sample B shows a broad band between 100 and 275 cm^{-1}, again with three peaks at about 116 cm^{-1} (3.4 $\pm$ 0.007 THz), 144 cm^{-1} (4.3 $\pm$ 0.020 THz) and 185 cm^{-1} (5.6 $\pm$ 0.26 THz). Since the thickness of the GST layer in sample B is the same as that in sample A, it is surprising that the 6.5 THz TO phonon of the InAs substrate is not also observed in sample B. From the Raman spectra of the two GST/InAs (111) samples we can say that at least three peaks appear to be associated with the GST in each sample. The first two peaks have about the same frequency in samples A and B, while the third peak appeared at different frequencies for samples A and B.

3. Discussion

The phonon frequencies extracted from the bare InAs(111) substrate and the two GST/InAs(111) samples are shown in Table 2, and include values obtained from R and AR signals as the pump polarisation was varied. The table shows the frequencies extracted from the pump-probe measurements by the different methods described previously. The values determined from the FFT power spectra agree well with fits to the TD data (described in the appendix) that assume no chirp, since both yield the average frequency of oscillation during the scan. The value obtained by fitting the time domain data with the chirp as a variable parameter effectively measures the instantaneous frequency at the beginning of the scan, immediately after excitation by the pump. Based upon the chirped fitting, an extrapolated frequency value is also stated that corresponds to the frequency at the end of the oscillation, when the sample temperature has fallen somewhat. This frequency was calculated by first subtracting the instantaneous frequency at the beginning of the scan from the frequency extracted from the FFT, and then adding this difference to the frequency extracted from the FFT. The value of this fourth frequency was approximately 3.4 THz for both GST/InAs(111) samples.

We begin by discussing the results from the micro-Raman measurements on the InAs(111) wafer. Raman selection rules [25] suggest that for the normal incidence scattering geometry both the TO and LO zone-centre phonon modes should be observed, the latter with a weaker intensity. The multi-peak fit of the Raman spectrum in Fig. 6(a) clearly indicates three peaks. In agreement with theory, the LO peak has a much lower intensity than the TO mode. The measured LO and TO frequencies match very well with the literature values (both experimental and theoretical). Being a polar material, the InAs wafer supports the Fuchs-Kliewer surface mode [26] with its frequency matched with those of the TO and LO modes in accordance with theory [25]. Interestingly, we find that the intensity of the Fuchs-Kliewer mode is intermediate to those of the TO and LO modes. As mentioned earlier, our pump-probe measurement of the TO mode frequency matches exactly with the micro-Raman measurement. The LO mode was not detected in the pump-probe experiment. Possible reasons for this are discussed later

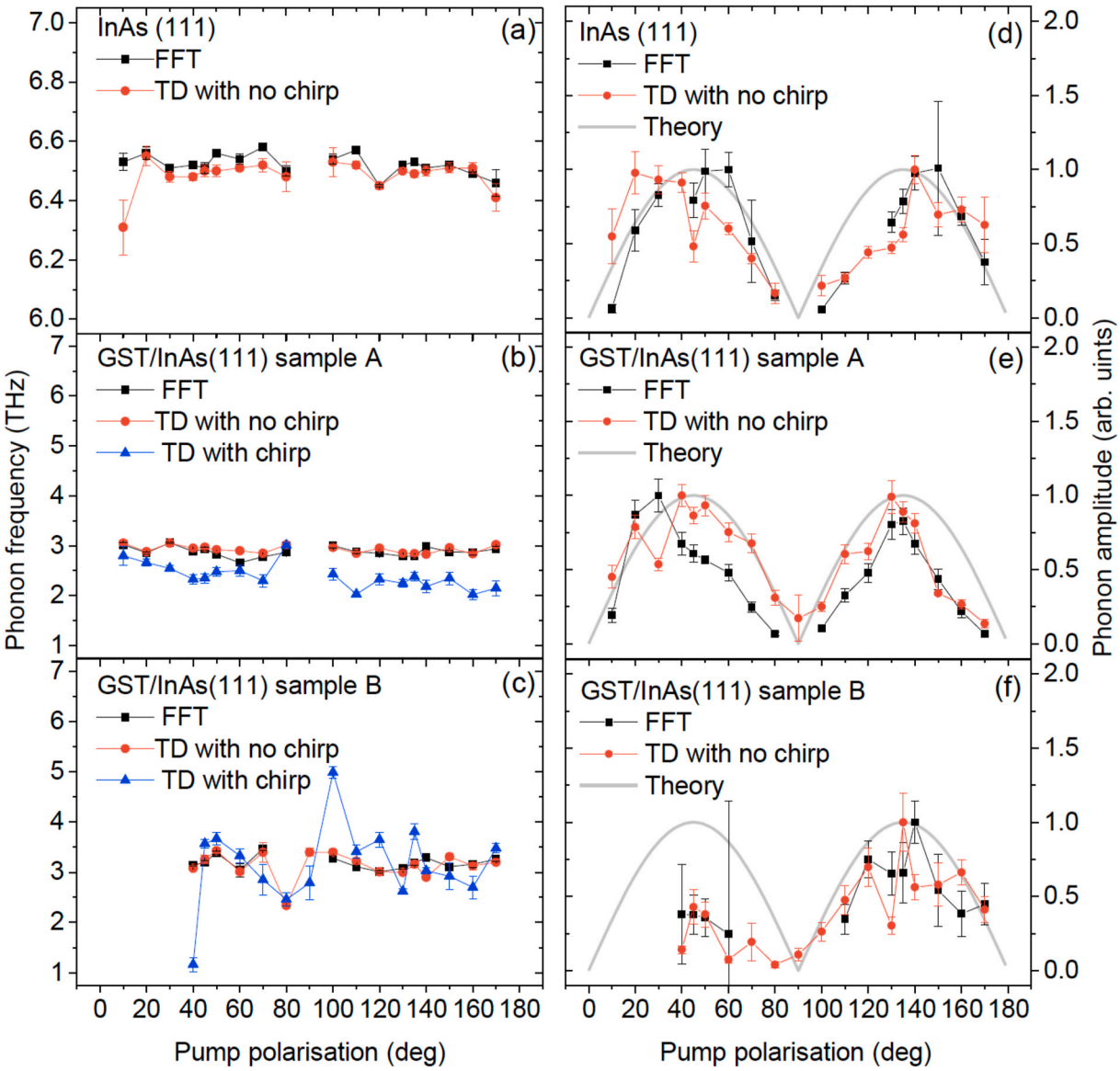

Fig. 3. Dependence of (left) oscillation frequency and (right) normalised amplitude upon angle of pump polarisation for the AR (ellipticity) signal obtained from (a) and (d) a bare InAs (111) substrate, (b) and (e) GST/InAs(111) sample A, and (c) and (f) GST/InAs(111) sample B. Values were obtained either directly from the power spectrum (FFT) of the experimental data, or fitting the time domain data, either without allowing for chirp (TD no chirp) or allowing for chirp (TD with chirp) in (b) and (c). The amplitude is plotted as a positive quantity and so the expected analytical form $|\sin(2(\theta-\varphi))|$ (grey curve) is plotted for comparison. In panels (c) and (f), for angles of 10–30°, the signal quality was insufficient for a frequency and amplitude to be extracted. The error bars were obtained from fitting the experimental data to the functions described within the main text and do not account for sources of systematic error such as drift in the overlap of pump and probe spots. Two outliers from the set of black data points have been excluded in both (d) and (f). An alternative version of the plot with the outliers included is provided within Supplementary Material.

when results for GST/InAs(111) are presented.

Next we discuss measurements on the GST/InAs(111) system. The extracted phonon frequencies for sample B are consistently higher by 0.1–0.2 THz compared to those for sample A, and oscillations were observed in the R signal from sample B but not A. Also, as mentioned earlier, the TO phonon of the InAs substrate was not detected for sample B. These facts point to structural differences between the two samples. Specifically, we speculate that the surface termination and step density were different for the InAs substrates for samples A and B, leading to differences in the structure of the GST epilayers. The frequencies of the lowest lying modes in the Raman measurements were 3.7 THz for sample A and 3.4 THz for sample B. Both values are greater than those extracted from the pump-probe measurements. This is probably because the pump-probe measurements are made at a higher temperature due to the heating by the pump, which causes softening of the lattice and a reduction of phonon frequency. A transient temperature profile was calculated previously [27] for a 20 nm thick crystalline GST film grown on a Si substrate, capped with a transparent layer, and pumped with 60 fs pulses of 800 nm wavelength and fluence of 2.33 mJ/cm^2. The temperature at the centre of the GST layer was found to increase to 700 K after 1 ps, so that a peak temperature of about 470 K might be expected for the fluence of 1 mJ/cm^2 used in Figs. 1–4 of the present work. We note also that the observed modes lie close to the edge of a high-pass filter designed to block elastically scattered light within the Raman measurements. Therefore, it is possible that the filter introduces some asymmetry into the shape of the lowest lying mode and hence also a small shift in its apparent frequency. Additionally, the transient temperature change could be different for samples A and B due to differences in the structural quality that affect both the optical absorption and thermal conduction from the excited region.

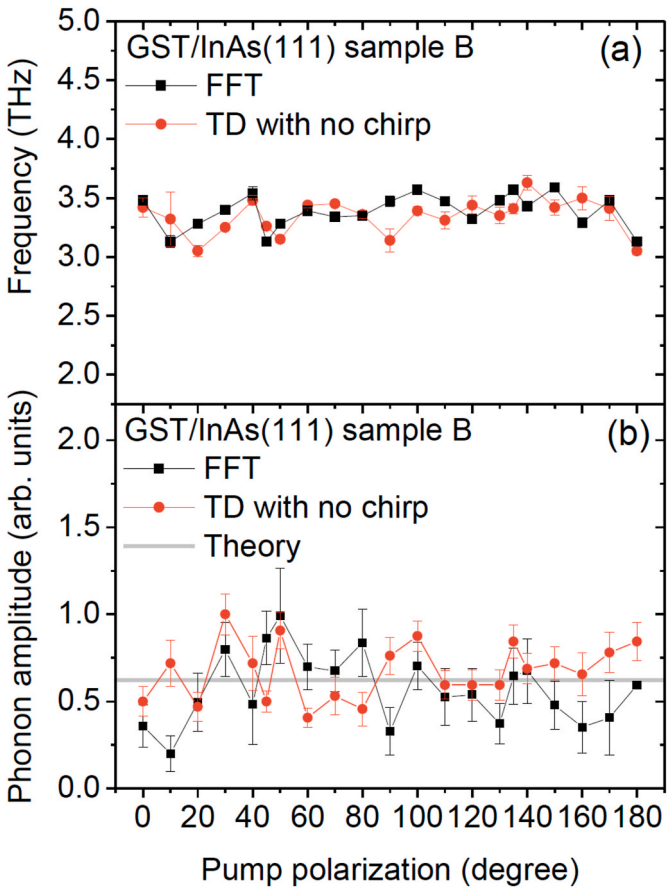

Fig. 4. Dependence of phonon (a) frequency and (b) amplitude upon pump polarisation extracted from the reflectivity (R) signal from GST/InAs(111) sample B.

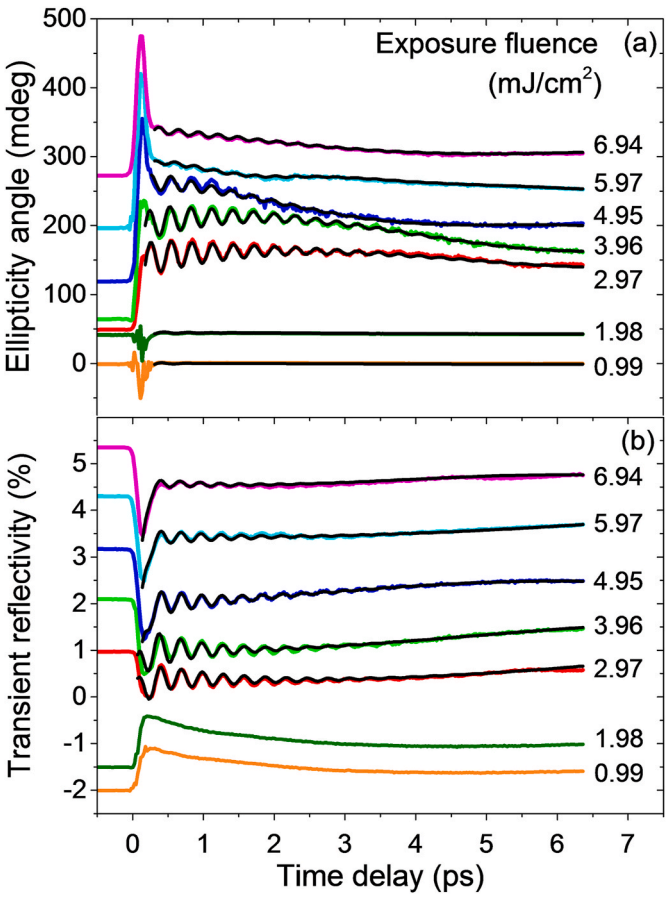

Fig. 5. Dependence of (a) transient ellipticity (AR) and (b) reflectivity (R) from sample A after exposure to elevated pump fluence when the pump and probe polarisations were set to lie 45° apart.

The TSRS theory suggests that the 6.5 THz phonon mode observed in the InAs(111) wafer is one of the three dimensional T_2 phonon modes, while the Raman spectra suggest that it is the TO phonon. Based on the TSRS theory, the appearance of a mode with 3.4 THz frequency in both transient R and AR (ellipticity) signals for one of the GST/InAs (111) samples suggests that it is a three-dimensional T_2-like mode. The presence of vacancies within the GST and the displacement of ions from their positions in the ideal rock-salt structure removes the inversion symmetry, allowing first order Raman scattering in micro-Raman measurements. The observation of the T_2-like phonon modes, at 6.5 THz and 3.4 THz, suggests that GST epilayers grown on InAs(111) have a rock-salt-like structure.

The experiments show that the phonon amplitude extracted from AR measurements of the InAs(111) wafer and both GST/InAs(111) samples has the $\sin(2(\theta - \varphi))$ dependence upon the pump and probe polarisation that is predicted by TSRS theory. This behaviour is characteristic of the specular optical Kerr effect (SOKE) but in fact confirms that the coherent optical phonons in InAs(111) and GST/InAs (111) are excited by the ISRS mechanism. The SOKE is a general phenomenon described by nonlinear susceptibility tensors without making assumptions about the underlying microscopic mechanisms [28]. Hence, the ISRS and the SOKE are seen to provide equivalent descriptions of the same phenomenon. The amplitude of the T_2-like mode is almost zero when the polarisations of the pump and probe are parallel or perpendicular to each other, suggesting that the SC mechanism does not contribute to the mode excitation.

In a previous study of GST/GaSb(001) [4], the TSRS theory was used to predict that, for the (001) surface of zinc blende or rocksalt, only the A and E modes should be observed in the R signal, with no dependence upon pump and probe polarisation. Only the T_{2z} mode should be observed in the AR signal with amplitude proportional to $\sin(2\varphi)\cos(2\theta)$, where θ and φ are defined relative to an in-plane cube edge. A long-lived oscillation exhibiting this angular dependence was indeed observed and attributed to a T_{2z} – like mode of the defective GST structure. For InAs (111), where a superposition of T_{2x}, T_{2y}, and T_{2z} modes is excited, long lived oscillations are observed. However, for the GST/InAs(111) samples, the oscillations are heavily damped and strongly chirped, so that the frequency increases with time delay. The larger damping may occur because GST has a defective structure in which the degeneracy of the T_{2x}, T_{2y}, and T_{2z} modes is lifted. Since the pump excites a superposition of these 3 modes, any splitting of their frequencies will lead to dephasing within the measured signals that will enhance the apparent damping.

The Raman spectra of both GST/InAs(111) samples are similar to those found in the literature [11,29–34]. The results can be compared and contrasted with those obtained previously for epitaxial GST films of (100) orientation [29]. The peaks observed for sample A in the present study are noticeably sharper than those observed for GST/GaSb(100), suggesting that films of (111) orientation may have superior structural quality. In that study two optical phonons were observed, one at 3.4 THz and the other at 4.5 THz. One possible explanation for the appearance of the peaks at 4.6 and 5.6 THz in the two GST/InAs(111) samples could be differences related to the growth conditions. Another possibility is that these modes are the GST/substrate interface modes. It is beyond the scope of this study to investigate these possibilities. The lowest frequency mode (3.4 THz) in each GST/InAs(111) sample was also observed in the pump-probe measurements as explained above, while the other two modes did not appear, most likely because they are not

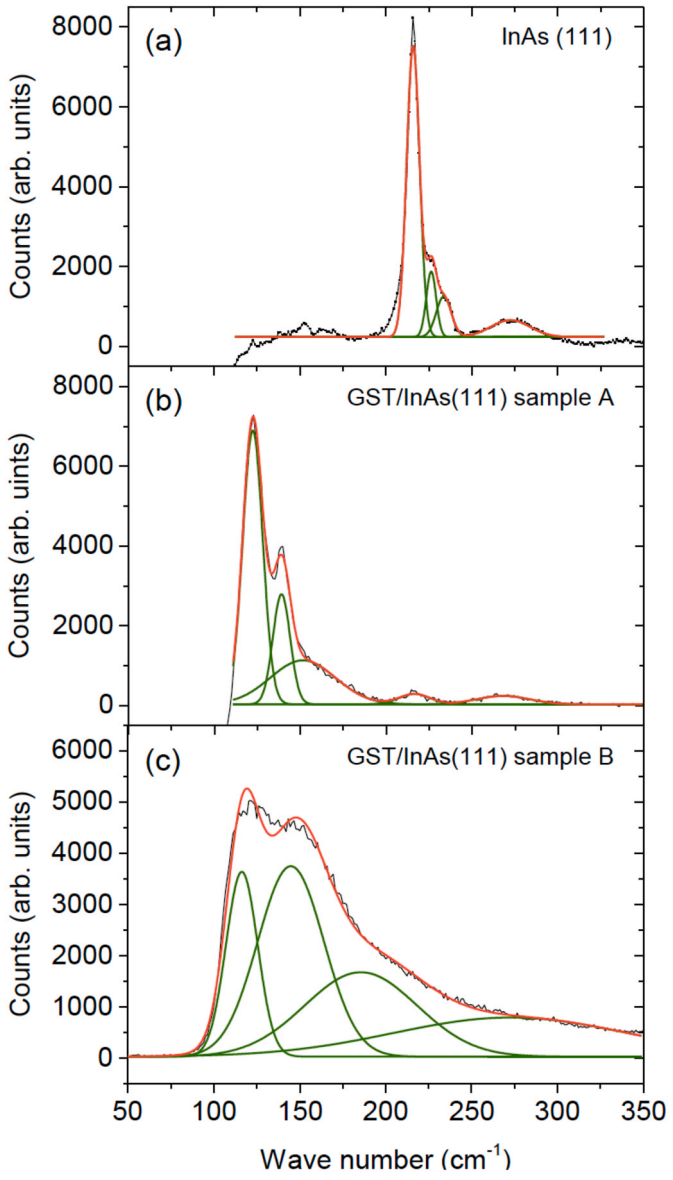

Fig. 6. Raman spectra obtained from (a) a bare InAs(111) substrate, (b) GST/InAs(111) sample A (c) GST/InAs(111) sample B. The black curves show the experimental data, the red curves represent multi-peak fits, while the green curves show the constituent peaks contributing to the multi-peak fits. (For interpretation of the references to colour in this figure legend, the reader is referred to the Web version of this article.)

observable on grounds of symmetry as discussed in the theory of TSRS that was presented previously. As the mode at 3.4 THz is detected for both GST/InAs(111) and GST/GaSb(001), it can be concluded that this COP is intrinsic to bulk GST and is unaffected by the substrate.

For the Raman spectra obtained from the InAs(111) wafer, both the TO and LO bulk phonons are observed while in the pump-probe measurements only the TO phonon is observed. The reason why the pump-probe measurement detects the TO phonon mode but not the LO phonon mode is not yet clear, but there are three possibilities. First, from calculations that consider the Raman selection rules for backscattering from the (111) wafer of the zinc blende structure, to detect both TO and LO phonon modes, the polarisation of the incident and scattered beams should lie in the same plane. In the pump-probe measurements two beams interact with different electric polarisations so perhaps the polarisation of the incident and scattered beams are not in the same plane, resulting in much reduced signal of the low-intensity LO Raman mode. Second, there may be some fundamental reason, based upon a more detailed microscopic treatment, for why a pump-probe signal from the LO phonon is forbidden. The third possibility could be instrumental, for example due to limited frequency resolution.

4. Conclusion

In summary, several optical phonon modes have been identified for $Ga_2Sb_2Te_5$/InAs(111) and InAs(111) from pump-probe and micro-Raman measurements. For a bare InAs(111) substrate, TSRS revealed a single mode with frequency of 6.5 THz that is identified as the T_2 transverse optical (TO) phonon, while RS in addition revealed the 7.0 THz longitudinal optical (LO) phonon and 6.8 THz Fuchs-Kliewer surface phonon. The amplitude of the TO mode observed in AR measurements is proportional to $\sin(2(\theta - \varphi))$, as predicted for both ISRS and the specular optical Kerr effect (SOKE), confirming that ISRS and SOKE are equivalent descriptions of the same phenomenon.

A single mode with frequency of about 3.4 THz and $\sin(2(\theta - \varphi))$ variation of amplitude was observed in AR measurements for both $Ge_2Sb_2Te_5$/InAs(111) samples, confirming the T_2-like character of the mode and hence the underlying cubic structure of the epilayer. A mode with frequency of 3.4 THz was observed in R measurements of sample B, but not for sample A, with amplitude that was independent of φ and θ as predicted by TSRS theory. The 3.4 THz R and AR signals were heavily damped in all cases, with typical relaxation time <1 ps, which may be attributed to dephasing of T_{2x}, T_{2y}, and T_{2z} modes that become non-degenerate due to structural distortions. After exposure to elevated pump fluence, large amplitude oscillations with frequency of 3.5 THz and relaxation time of 1.5 ps were observed in both R and AR signals for sample A, while the response of sample B remained largely unchanged. RS measurements revealed modes at 3.7, 4.2 and 4.6 THz in sample A and at 3.4, 4.3, and 5.6 THz in sample B. Taken together, the TSRS and RS measurements suggest that the nominally similar epilayers in samples A and B may possess subtle differences in structure (in the GST layers or at the GST/substrate interface) that have significant influence upon their phonon spectrum. Further work is required to characterise these differences and correlate them with the observed phonon spectra. As the 3.4 - 3.7 THz mode is detected for both GST/InAs(111) and GST/GaSb(001), it is concluded to be a COP intrinsic to the bulk form of the phase change material GST.

Table 2
Frequencies in THz of the lowest lying phonon modes of the InAs(111) wafer and the two GST/InAs(111) samples extracted from time resolved R and AR signals in pump-probe measurements, and micro Raman measurements. Frequencies were extracted from pump-probe measurements using different methods: fitting a Lorentzian curve to the FFT power spectrum; fitting a sinusoid to the TD data assuming no chirp; fitting the TD data allowing for chirp; and using the values from the previous two methods to extrapolate to long time delays.

		InAs(111)		GST/InAs(111) sample A				GST/InAs(111) sample B			
Pump-probe	Signal	FFT	TD no chirp	FFT	TD no chirp	TD with chirp	TD long delay	FFT	TD no chirp	TD with chirp	TD long delay
	S_{AR}	6.51 ± 0.002	6.495 ± 0.005	2.897 ± 0.025	2.925 ± 0.017	2.380 ± 0.073	3.41	3.18 ± 0.03	3.03 ± 0.06	3.06 ± 0.17	3.3
	S_R	–	–	–	–	–	–	3.32 ± 0.02	3.37 ± 0.02	–	–
Micro-Raman		6.5 ± 0.003		3.7 ± 0.001				3.4 ± 0.007			

Data availability

The data that support the findings of this study are available from the corresponding author upon reasonable request.

Acknowledgments

The authors gratefully acknowledge the assistance of Dr P. S. Keatley in producing the final versions of the figures and the financial support of the UK Engineering and Physical Sciences Research Council grant EP/F015046/1.

Appendix A. Supplementary data

Supplementary data to this article can be found online at https://doi.org/10.1016/j.ssc.2022.114788.

Appendix: Fitting procedure

Typically the time resolved ellipticity (AR) signals obtained from the samples in this study can be divided into three regimes in terms of the delay time t_d between the pump and probe pulses. In the first region, $t_d < 0$, where the probe pulse reaches the sample before the pump pulse, the reflected probe beam does not record any change in the sample response. The second region occurs around $t_d = 0$, where the pump and probe pulses overlap and a large peak is seen in the signal due to the specular optical Kerr effect (SOKE). The last region occurs for $t_d > 0$ when the pump arrives before the probe. Typically an oscillatory component associated with a coherent optical phonon is superimposed upon an exponential background.

The ellipticity (AR) signal can generally be fitted by a function that is a superposition of a Gaussian peak, a damped oscillation, and a simple exponential decay term. Assuming that both pump and probe pulses have Gaussian temporal profile, the normalised intensity of the pump beam can be written as

$$I(t) \propto \frac{1}{\sqrt{2\pi}w} exp\left(\frac{-t_d^2}{2w^2}\right), \tag{A1}$$

where w determines the width of the pulse. In principle the dependence of the ellipticity signal upon the time delay can be calculated from a double convolution of the Gaussian pump and probe pulses with the system response. With this in mind, a suitable fitting function is

$$\begin{aligned} S_{AR} \propto & A exp\left(\frac{t_d^2}{4w^2}\right) \\ & + \frac{B}{2} exp\left(\frac{w^2}{t_1^2} - \frac{t_d}{t_1}\right)\left[1 - erf\left(\frac{w}{t_1} - \frac{t_d}{2w}\right)\right] \\ & + \sum_i \frac{C_i}{2} \exp\left(\frac{t_d}{t_{2i}}\right) \\ & \times \left[1 + erf\left(\frac{t_d}{2w}\right)\right] cos\left[2\pi f_i t_d + 2\pi\beta_i t_d^2 + \varphi_i\right]. \end{aligned} \tag{A2}$$

The first term with amplitude A assumes that the system response is a Dirac delta function. It represents the instantaneous incoherent sample response and is used to fit the SOKE peak within the ellipticity signal. The second term with amplitude B assumes that the system response is an exponential decay with time constant t_1, where erf is the Gaussian error function. It is used to fit the exponential background within the signal. The third term is phenomenological and can describe a number of oscillatory terms, with amplitude C_i, frequency of oscillation, f_i, damping time t_{2i}, initial phase of oscillation φ_i, and with chirp determined by the parameter β_i. This term represents the damped oscillatory response of a phonon mode to the pump pulse with the chirp parameter being used to describe any changes in the phonon frequency with time due to changes in the temperature. A constant offset term may also arise, either from diffuse scatter of the pump pulse, or because the system cannot fully relax between successive pump pulses.

Fitting all features within the signal simultaneously can be arduous due to the large number of variable parameters involved. Therefore just the exponential decay and oscillatory components of the signal were fitted, from a value of t_d at which the SOKE peak no longer had significant amplitude. In general two oscillatory components ($i = 1,2$) were required to fit the data, one of THz frequency and the other of GHz frequency. The fitting was carried out in two steps. Firstly, the raw time resolved data was fitted after setting the chirp parameter β_i to 0 and the pulse width to 100 fs? The oscillatory signal components were then isolated by subtracting the fitted exponential relaxation background term. At this point the frequency of the THz mode contained within the oscillatory residual was extracted from a fast Fourier transform (FFT). The peak in the FFT was fitted to a Lorentzian curve of form

$$y = y_\circ + \left(\frac{2A}{\pi}\right)\left[\frac{\Delta x}{(x - x_c)^2 + (\Delta x)^2}\right]$$

in which y_0 is a constant offset value, A is the area under graph, Δx is the full width of the peak at half height, and x_c is the centre frequency of the peak. The oscillatory residual was then fitted again using the second and third terms in equation (A2). The initial frequency of the THz mode was set equal to that obtained from the FFT, and the chirp parameter was allowed to vary so as to describe any change in the phonon frequency with time. The ellipticity signal of the bare InAs(111) substrate did not exhibit any clear chirp, therefore the fitting process involved just the first step described above.

References

[1] D. Lencer, M. Salinga, M. Wuttig, Adv. Mater. 23 (2011) 2030.
[2] A.V. Kolobov, P. Fons, A.I. Frenkel, A.L. Ankudinov, J. Tominaga, T. Uruga, Nat. Mater. 3 (2004) 703.
[3] X.Q. Liu, X.B. Li, L. Zhang, Y.Q. Cheng, Z.G. Yan, M. Xu, X.D. Han, S.B. Zhang, Z. Zhang, E. Ma, Phys. Rev. Lett. 106 (2011), 025501.

[4] A. Shalini, Y. Liu, U.A.S. Al-Jarah, G.P. Srivastava, C.D. Wright, F. Katmis, W. Braun, R.J. Hicken, Sci. Rep. 3 (2013) 2965.
[5] M. Först, T. Dekorsy, C. Trappe, M. Laurenzis, H. Kurz, B. Béchevet, Appl. Phys. Lett. 77 (2000) 1964.
[6] J. Hernandez-Rueda, S.A. Avoia, W. Gawelda, J. Solis, B. Mansart, D. Boschetto, J. Siegel, Appl. Phys. Lett. 98 (2011) 251906.
[7] V. Bragaglia, K. Holldack, J.E. Boschker, F. Arciprete, E. Zallo, T. Flissikowski, R. Calaraco, Sci. Rep. 6 (2016) 28560.
[8] Y. Li, V.A. Stoica, L. Endicott, G. Wang, C. Uher, R. Clarke, Appl. Phys. Lett. 97 (2010) 171908.
[9] K. Makino, J. Tominaga, A.V. Kolobov, P. Fons, M. Hase, Appl. Phys. Lett. 101 (2012) 232101.
[10] M. Hase, Y. Miyamoto, J. Tominaga, Phys. Rev. B 79 (2009) 174112.
[11] G.C. Sosso, S. Caravati, R. Mazzarello, M. Bernasconi, Phys. Rev. B 83 (2011) 134201.
[12] J.E. Boschker, X. Lü, V. Bragaglia, R. Wang, H.T. Grahn, R. Calarco, Sci. Rep. 8 (2018) 5889.
[13] V. Bragaglia, A. Schnegg, R. Calarco, K. Holldack, Appl. Phys. Lett. 109 (2016) 141903.
[14] V. Bragaglia, A. Schnegg, R. Calarco, K. Holldack, Epitaxial GeTe-Sb2Te3 alloys probed by single cycle THz pulses of coherent synchrotron radiation, in: Light, Energy and the Environment, OSA Technical Digest (Online), Optical Society of America, 2016 paper FW3D.3.
[15] T. Dekorsy, G.C. Cho, H. Kurz, Coherent phonons in condensed media, in: M. Cardona, G. Güntherodt (Eds.), Light Scattering in Solids VIII. Topics in Applied Physics, vol. 76, Springer, Berlin, Heidelberg, 2000.
[16] R. Merlin, Solid State Communications, 102, 1997, p. 207.
[17] The vector group theoretical representation of the zone-centre optical phonons of the rock-salt structure is T_1. However, as in the previous work [4], we have used the label T_2 for the sake of consistency.
[18] F. Katmis, R. Calarco, K. Perumal, P. Rodenbach, A. Giussani, M. Hanke, A. Proessdorf, A. Trampert, F. Grosse, Shayduk Roman, R. Campion, W. Braun, H. Riechert, Cryst. Growth Des. 11 (2011) 4606.
[19] R. Calarco, A.V. Kolobov, P. Fons, A. Giussani, P. Rodenbach, K. Perumal, M. Krbal, Spring-8/SACLA Res. Rep. 3 (2015) 10, https://doi.org/10.18957/rr.3.1.10.
[20] J.E. Boschker, J. Momand, V. Bragaglia, R. Wang, K. Perumal, A. Giussani, B. J. Kooi, H. Riechert, R. Calarco, Nano Lett. 14 (2014) 3534.
[21] V. Bragaglia, F. Arciprete, A.M. Mio, R. Calarco, J. Appl. Phys. 123 (2018) 215304.
[22] E. Zallo, S. Cecchi, J.E. Boschker, A.M. Mio, F. Arciprete, S. Privitera, R. Calarco, Sci. Rep. 7 (2017) 1466.
[23] V. Bragaglia, F. Arciprete, W. Zhang, A. Massimiliano Mio, E. Zallo, K. Perumal, A. Giussani, S. Cecchi, J.E. Boschker, H. Riechert, S. Privitera, E. Rimini, R. Mazzarello, R. Calarco, Sci. Rep. 6 (2016) 23843.
[24] V. Bragaglia, B. Jenichen, A. Giussani, K. Perumal, H. Riechert, R. Calarco, J. Appl. Phys. 116 (2014), 054913.
[25] P. Yu, M. Cardona, Fundamentals of Semiconductors", Springer-Verlag Berlin Heidelberg, 2010.
[26] R. Fuchs, K.L. Kliewer, Phys. Rev. 140 (1965) A2076.
[27] Y. Liu, M.M. Aziz, A. Shalini, C.D. Wright, R.J. Hicken, J. Appl. Phys. 112 (2012) 123526.
[28] Yu P. Svirko, N.I. Zheludev, Polarization of Light in Nonlinear Optics, Wiley, New York, 1998.
[29] A. Shalini, Y. Liu, F. Katmis, W. Braun, G.P. Srivastava, R.J. Hicken, J. Appl. Phys. 117 (2015), 025306.
[30] B. Liu, Z.-T. Song, T. Zhang, S.-L. Feng, B. Chen, Chin. Phys. 13 (2004) 1947.
[31] E. Cho, S. Yoon, H.R. Yoon, W. Jo, J. Kor. Phys. Soc. 48 (2006) 1616.
[32] P. Nemec, V. Nazabal, A. Moreac, J. Gutwirth, L. Benes, M. Frumar, Mater. Chem. Phys. 136 (2012) 935.
[33] W. Braun, R. Shayduk, T. Flissikowski, M. Ramsteiner, H. Grahn, H. Riechert, P. Fons, A. Kolobov, Appl. Phys. Lett. 94 (2009), 041902.
[34] J. Akola, R.O. Jones, J. Phys. Condens. Matter 20 (2008) 465103.